Magnetization reversal dynamics in ultrathin magnetic layers

B. Raquet, R. Mamy, and J. C. Ousset
Laboratoire de Physique des Solides et Service National des Champs Magnetiques Pulsés, INSA Complexe Scientifique de Rangueil, 31077 Toulouse Cedex, France
(Received 29 February 1996)

We propose an analytical expression of the magnetization reversal in ultrathin magnetic layers, modeling the after effects, and taking into account both domain-wall motion and nucleation processes. We apply our modelization to quantify the dynamical properties of the magnetization of MoS_2/Au/Co/Au sandwiches; we define the Barkhausen volume, the wall velocity, and the nucleation rate depending on the applied magnetic field and the radius and the density of nuclei sites on the surface of the sample. Finally, we investigate an original behavior of the switch of the magnetization in high dynamic regime. An attempt is made to explain the divergence of the coercive field in large field variation rates (dH/dt), by introducing both the thermally activated and the viscous processes driving the wall motion. [S0163-1829(96)06630-1]

I. INTRODUCTION

Current research on the ultrathin magnetic layers is largely focused on the magnetic domain structure and the mechanisms of the magnetization reversal. These studies are driven by fundamental interests (the origins and the shape of magnetic domains, the understanding of the coercive field value governed by the nucleation process and domain-wall displacements, the dynamical magnetization, and the link with the nanocrystallographic structure . . .) and technical applications in the information storage media such as higher recording density, stability, and improvement of magnetic bits . . . .

During the last years, in some ultrathin film cases, such as Co/Au,[1–3] Co/Cu,[4] Ni/Cu,[5] means of magnetic visualization as magnetic force microscopy, scanning electron microscopy with polarization analysis, or Faraday microscopy confirm unambiguously the stability of a multidomain magnetic structure in zero field and its mobility when an external field is applied. These observations are correlated, with a good agreement, to theoretical calculations predicting the formation and the size of bubble and stripe domains varying with the magnetic layer thickness, the exchange interactions and the magnetic anisotropy.[5,6] Thus, it would be an unrealistic assumption to consider that the magnetization reversal might be modelized assuming the ultrathin film as a single magnetic domain. Therefore, the understanding of the magnetization switch and its dynamic imply the quantification of the nucleation and the wall motion processes depending on the applied magnetic field (H) and its variation rate (dH/dt). Previous works[7,8] developed a phenomenological model of dynamical properties of the magnetization reversal; the calculations were based on the definition of a macroscopic relaxation time linked to thermally activated mechanisms: they considered, separately, either a single domain-wall displacement, either a switch of microdomains, according to the main process of magnetization (respectively the propagation of domains or the nucleation).

The objective of this paper is to present an original and general modelization of the hysteresis loops which allows to consider simultaneously the dynamical effects and the complex competition between domain nucleations and domain-wall motions. This modelization allows us to deduce a general analytical expression of the magnetization $M[H,(dH/dt)]$ describing all multidomain reversal processes based on intrinsic and microscopic parameters: the Barkhausen volume, the nucleation rate $R(H)$, the wall velocity $V(H)$, the radius r_c, and the total number of nuclei sites N_0 on the surface of the sample. This model is based on the calculation of expanding areas with a variable magnetic field, simulating the birth and the growth of the magnetic domains through the magnetic layer.

In Sec. II, the general expression of the magnetization $M(H,dH/dt)$ is derived. Section III is devoted to improve the physical validity of the model owing to several simulations: the results emphasize the strong influence of the previously listed parameters on the shape of the hysteresis loop and the coercive field value. Finally, in Sec. IV, we apply this theoretical approach to characterize the magnetization processes in a model magnetic system: the Au/Co/Au sandwiches. Surface magneto-optical polar Kerr-effect measurements, with a field variation rate up to 1.2 MOe s^{-1}, were performed at room temperature on two typical Au/Co/Au samples, grown on MoS_2 with different conditions. We shall stress that the dynamical study of the magnetization, correlated to our modelization, allows a precise and quantitative analysis of the magnetic properties of the magnetization switch of the cobalt layer. We also propose an extension of our calculation to describe an original dynamical behavior of the magnetization that we observed recently;[8] our approach attempts to explain that the experimental divergence of the coercive field, in a high-field variation rate, occurs via the domain-wall dynamics and the nucleation process.

II. DERIVATION OF THE DYNAMICAL MAGNETIZATION EQUATION

Calculations are intended to find an analytical expression of the magnetization $M(H,dH/dt)$, giving a description of a multidomain reversal process of the magnetization in an ultrathin magnetic layer. First of all, the methodological approach is based on a mathematical calculus of areas corre-

sponding to the nucleation centers and the propagation of domain walls. This model is developed in the light of the Fatuzzo's theory[9] concerning the relaxation of the polarization reversal in Ferro-electrical crystal. Recently, Fatuzzo's equation was applied by Labrune[10] to express the relaxation of the magnetization of an ultrathin magnetic film. The most fundamental difference between Fatuzzo-Labrune's theories and our model, is to consider a variable magnetic field applied to the magnetic layer and not a constant electric or magnetic field as in Refs. 9 and 10. It means that magnetization dependence on the magnetic field H and its variation rate (dH/dt) have to be considered; the calculation steps are tedious but finally, we shall demonstrate that resulting expression $M[H,(dH/dt)]$ is simple and allows us to fit experimental magnetization measurements.

To consider the delicate overrunning of nucleations and the coalescence of domains due to their sideways expansions, we first calculate the global switched area $A[H,(dH/dt)]$, neglecting the possible overlap. Then, applying the Avrami's theorem,[11] the real area called $\Theta[H,(dH/dt)]$, corresponding to the magnetization switched by the field, can be deduced from the following expression:

$$\Theta[H,(dH/dt)]=1-\exp\{-A[H,(dH/dt)]\}. \tag{1}$$

Therefore, the magnetization is given by

$$M[H,(dH/dt)] = M_S[-2(1-\exp\{-A[H,(dH/dt)]\})+1]. \tag{2}$$

A. Switched area $A[H,(dH/dt)]$

We calculate the switched area in a negative field and neglect the possible overrunning of domains. We assume that domains are born at random on the sample surface according to a statistical process and go across the whole thickness of the magnetic layer.[9,12] It is defined by the nucleation rate $R(H)$ per unit of time and depending on the applied magnetic field.

Let us consider N_0 the total number of the nuclei centers (i.e., the total number of nucleation that can be formed on the sample) and $N[H,(dH/dt)]$, the number of domains appeared at the applied field $H,\{N[H,(dH/dt)]\leqslant N_0\}$. Then, the differential equation giving $N[H,(dH/dt)]$, in a negative field, can be written as

$$\frac{dN[H,(dH/dt)]}{\{N_0-N[H,(dH/dt)]\}}=\frac{R(H)dH}{(dH/dt)}. \tag{3}$$

Straightforward integration gives

$$N[H,(dH/dt)]=N_0\left\{1-\exp\left(-\frac{1}{(dH/dt)}\int_0^H R(H)dH\right)\right\}. \tag{4}$$

We assume that, once born, the nucleation might expand sideways by radial motion defined by a radius $r(H)$ and a radial velocity $V(H)$, varying with the applied magnetic field. Let us suppose a nucleation born in a negative field H_1, $0>H_1>H$, the switched area by expansion of its center in a field H, called $\sigma(H)_{H_1}$, is assumed to be given by

$$\sigma(H)_{H_1}=\frac{\pi}{1}[r(H)_{H_1}+r_c]^2-\frac{\pi r_c^2}{T}, \tag{5}$$

where $r(H)_{H_1}$ is the grown radius in a field H, for a nucleus site appeared in a field H_1 (T is the global area to be reversed; for the numerical applications, we assume this area to be equal to the surface of the laser beam on the sample $-0.01\ \mathrm{cm}^2-$), one obtains

$$r(H)_{H_1}=\int_{H_1}^{H}V(H)\frac{dH}{(dH/dt)}. \tag{6}$$

If we assign the above area to the total number of nucleations born between zero field and H, the switched area $A(H,dH/dt)$ can be calculated by the following expression:

$$A[H,(dH/dt)]=\int_0^H\left.\frac{dN[H,(dH/dt)]}{dH}\right|_{H_1}\times\sigma(H)_{H_1}dH_1 + N[H,(dH/dt)]\frac{\pi r_c^2}{T}. \tag{7}$$

The first term is the reversed area by the sideways growth of the magnetic domains. $dN[H,(dH/dt)]/dH|_{H_1}$ represents the instantaneous number of reversed nanodomains in a field H_1. The last term is the area covered by the nuclei sites at their birth.

From Eq. (4), we find that

$$\left.\frac{dN[H,(dH/dt)]}{dH}\right|_{H_1}=\frac{N_0R(H_1)}{(dH/dt)}\times\exp\left(-\frac{1}{(dH/dt)}\int_0^{H_1}R(H)dH\right). \tag{8}$$

Replacing in Eq. (7) and rearranging the terms, one obtains

$$A[H,(dH/dt)]=\frac{N_0\pi}{(dH/dt)T}\int_0^H R(H_1)\times\exp\left(-\frac{1}{(dH/dt)}\int_0^{H_1}R(H)dH\right)\times\left(\int_{H_1}^{H}\frac{V(H)}{(dH/dt)}dH+r_c\right)^2dH_1. \tag{9}$$

We assume that the elementary mechanisms of the reversal magnetization are thermally activated processes;[13–15] thus, the nucleation rate and the wall motion can be expressed as follows:

$$R(H)=r_0\exp\left[-\left(\frac{E_n+HM_sV_n}{kT}\right)\right], \tag{10}$$

$$V(H)=v_0\exp\left[-\left(\frac{E_p+HM_sV_p}{kT}\right)\right],\quad \text{in a negative field.} \tag{11}$$

E_n and E_p are the activation energy in zero field, related respectively to the blocking of the nucleus reversal and the

pinning strength of the wall. V_n and V_p are activation volumes, supposed to be identical to an elementary volume V, called the Barkhausen volume.[8,10,15] Equations (10) and (11) imply a single energy barrier for each mechanism. It is possible to introduce here some distribution of the activation energies and the Barkhausen volume to simulate some inhomogeneities in the magnetic layer. In the following calculation, we make the choice of a single activation energy and an average elementary volume to simplify the analytical expressions. We found these assumptions to be sufficient to fit our experimental data.

Let us write Eqs. (10) and (11) as follows:

$$R(H)=R_0\exp(-\beta VM_sH) \tag{12}$$

and

$$V(H)=V_0\exp(-\beta VM_sH), \tag{13}$$

R_0 and V_0 are, respectively, the nucleation rate and the velocity of the wall in zero field and $\beta=1/kT$. Using Eqs. (12) and (13) in Eq. (9) and after integrations, the following equation is obtained:

$$\begin{aligned}A[H,(dH/dt)]=&\frac{N_0\pi R_0}{(dH/dt)T}\int_0^H\exp(-\beta VM_sx)\\&\times\exp\left(\frac{R_0}{\beta(dH/dt)VM_s}\right.\\&\left.\times[\exp(-\beta VM_sx)-1]\right)\\&\times\left(-\frac{V_0}{\beta VM_s(dH/dt)}[\exp(-\beta VM_sH)\right.\\&\left.-\exp(-\beta VM_sx)]+r_c\right)^2dx.\end{aligned} \tag{14}$$

B. Analytical expression of the magnetization $M[H,(dH/dt)]$

From Eqs. (2) and (14), a tenuous calculation allows to define an analytical formula of the magnetization without any mathematical approximation. Only the main steps of the development, useful for the understanding, are presented here. Let us define:

$$a=-\beta VM_s,\quad b=\frac{R_0}{\beta(dH/dt)VM_s},$$

$$c=-\frac{V_0}{\beta(dH/dt)VM_s},\quad d=\exp(-\beta VM_sH),\quad e=r_c. \tag{15}$$

We substitute these expressions in Eq. (14) and it yields the following expression of the integral:

$$\begin{aligned}I[H,(dH/dt)]=&\int_0^H\exp(ax)\exp\{b[\exp(ax)-1]\}\\&\times\{c[d-\exp(ax)]+e\}^2dx.\end{aligned} \tag{16}$$

After successive integrations and term rearrangement, Eq. (16) is reduced to

$$\begin{aligned}I[H,(dH/dt)]=&(\exp\{b[\exp(aH)-1]\}-1)\\&\times\frac{1}{ab^3}(e^2b^2+2bce+2c^2)\\&-\frac{1}{ab^3}(b^2c^2-2c^2b-2dc^2b^2-2ceb^2\\&+b^2c^2d^2+2cedb^2+2dc^2b).\end{aligned} \tag{17}$$

We now introduce the following parameters:

$$x=\beta VM_sH,\quad dx/dt=\beta VM_sdH/dt,$$

$$k=\frac{V(H)}{r_cR(H)}=\frac{V_0}{r_cR_0},\quad \alpha=\frac{\pi r_c^2N_0}{T}. \tag{18}$$

x and dx/dt are, respectively, called the reduced field and the reduced field variation rate. The parameters k and α correspond to those defined by Labrune;[10] k characterizes the competition between the wall motion and the nucleation [in a first approximation, a predominance of wall motion (nucleation) implies $k\gg1$ (respectively, $k\ll1$)]. α represents the density of nuclei sites, neglecting the possible overlaps.

Fortunately, using Eq. (5) and substituting Eq. (18) in Eqs. (17) and (14), the analytical expression of the area $A[x,(dx/dt)]$ is given by the simple equation:

$$A[x,(dx/dt)]=2\alpha k^2\left\{\begin{aligned}&\frac{N[x,(dx/dt)]}{N_0}\left(1-\frac{1}{k}+\frac{1}{2k^2}\right)+\frac{R_0}{(dx/dt)}[\exp(-x)-1]\left(1-\frac{1}{k}\right)\\&+\frac{R_0^2}{2(dx/dt)^2}[\exp(-x)-1]^2\end{aligned}\right\}. \tag{19}$$

From a physical point of view, let us note an interesting boundary condition of Eq. (19): for a negligible wall motion ($k\to0$) and in a high negative field (to reach the magnetic saturation), the real switched surface is reduced to $\Theta\approx1-\exp(-\alpha)$. It means that, for any α value, the fundamental condition is respected: $\Theta\leqslant\alpha$. The total switched area must be smaller than the total area of nucleation sites, neglecting their overlap.

Finally, referring to Avrami's theorem[11] and Eq. (19), we obtain the general analytical expression of the magnetization, in a negative magnetic field, considering the nucleation, the wall motion and the dynamic of the applied field:

$$\frac{M[x,(dx/dt)]}{M_s} = -2\left(1-\exp\left\{-2\alpha k^2\left[\frac{N[x,(dx/dt)]}{N_0}\left(1-\frac{1}{k}+\frac{1}{2k^2}\right)+\frac{R_0}{(dx/dt)}[\exp(-x)-1]\left(1-\frac{1}{k}\right)+\frac{R_0^2}{2(dx/dt)^2}[\exp(-x)-1]^2\right]\right\}\right)+1. \quad (20)$$

Magnetization is defined by five fundamental and intrinsic parameters: $R_0=R(H=0)$, the nucleation rate in zero field, $V_0=V(H=0)$ is the wall velocity in zero field, V is the Barkhausen volume, N_0 is the total number of the nuclei sites, r_c is the radius of the nucleation.

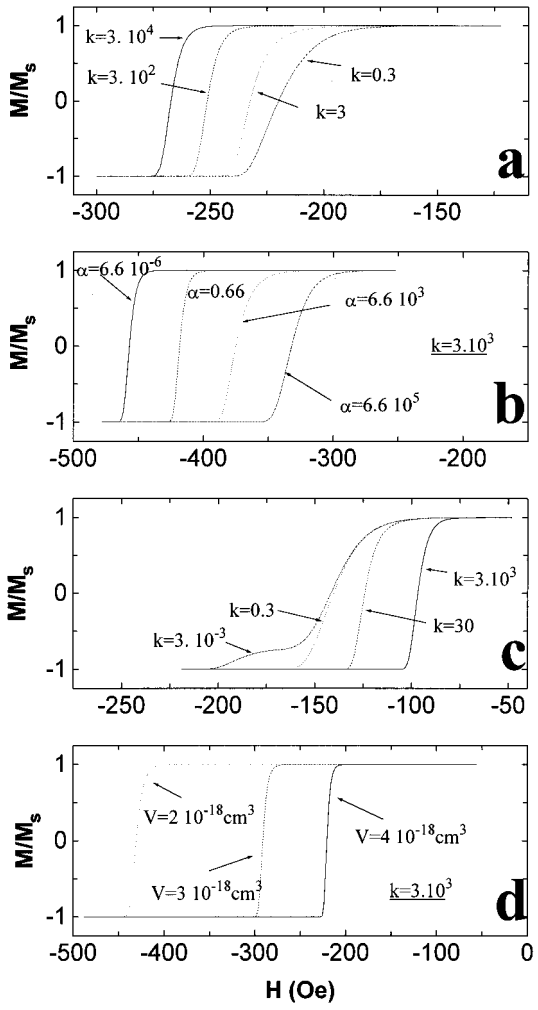

FIG. 1. Variation of $M(H,dH/dt)$ versus typical values of R_0, N_0, V_0, and V for thin magnetic films. (a) $V_0=10^{-13}$ cm/s, $r_c=3.25\times10^{-6}$ cm, $N_0=2\times10^8$, $V=3\times10^{-18}$ cm^3 for several values of R_0 ($R_0=10^{-12,-10,-8,-7}$ s^{-1}) corresponding to $k=3\times10^4$, 3×10^2, 3, and 0.3; (b) $R_0=10^{-18}$ s^{-1}, $V_0=10^{-20}$ cm/s, $r_c=3.25\times10^{-6}$ cm, $V=3\times10^{-18}$ cm^3 for several values of N_0 ($N_0=2.10^{3,8,12,14}$) corresponding to $\alpha=6\times10^{-6}$, 0.6, 6×10^3, and 6×10^5; (c) $R_0=10^{-4}$ s^{-1}, $N_0=6\times10^8$, $r_c=3.25\times10^{-6}$ cm, $V=3\times10^{-18}$ cm^3 for several values of V_0 ($V_0=10^{-6,-8,-10,-12}$ cm/s) corresponding to $k=3\times10^3$, 30, 0.3, and 3×10^{-3}; (d) $R_0=10^{-13}$ s^{-1}, $V_0=10^{-15}$ cm/s, $r_c=3.25\times10^{-6}$ cm, $N_0=2\times10^{-8}$ for several values of V ($V=4\times10^{-18}$, 3×10^{-18}, 2×10^{-18} cm^3).

The three first parameters allows us to express the nucleation rate $R(H)$ and the velocity $V(H)$ in a negative field, using Eqs. (12) and (13). Using R_0, V_0, and r_c, we deduce the ratio k to estimate the main reversal mechanism; finally, the Barkhausen volume is related to the interfacial length between pinning centers and N_0 could correspond to some specific defects responsible for the nucleation (like atomic steps in the magnetic layer).

III. SIMULATION OF THE MAGNETIZATION REVERSAL

To improve the potentiality of our model, we first propose an academic approach which consists of studying the variation of $M[H,(dH/dt)]$ versus typical values of V, R_0, V_0, and N_0. Figure 1 shows the drastic dependence of the magnetization [calculated by Eq. (20)] on the values of R_0 [Fig. 1(a)], N_0 [Fig. 1(b)], V_0 [Fig. 1(c)], and V [Fig. 1(d)]. For example, we notice that increase in the nucleation rate modifies the magnetic transition $+M_S/-M_S$ [Fig. 1(a)]: the more predominant the nucleation rate becomes, compared to the wall motion, the more the coercive field decreases and the more the transition is smooth; we find here a classical result describing the slope of the magnetic transition versus the main reversal process.[2,8,16] In Fig. 1(b), we show that the generally unknown value N_0 may induce large modifications on the hysteresis loop: whatever the value of the nucleation rate, few nuclei sites in the magnetic layer tend to favor the wall motion process. Figure 1(c) shows the variation of the magnetization reversal when the wall motion becomes less efficient compared the nucleation. The last curve (corresponding to $k\cong3\times10^{-3}$) is an interesting case; it shows that the magnetization can reverse in two steps when the two processes are energetically uncoupled enough: the first step related to the major part of the reversal is only due to the nucleation, but because of the low velocity, if the total number of nuclei sites cannot recover all the area of the sample, the nucleation process cannot reverse by itself the magnetization. That is why, we have to reach a higher field to activate the wall motion and complete the switch of the magnetization. Finally, Fig. 1(d) confirms that Barkhausen volume is a very sensitive and delicate value to define the width of the loop: little volumes need more energy to be reversed, it could be correlated to a higher density of magnetic defects in the interfaces.

Those simulations confirm that the shape of the hysteresis loop and the coercive field value depend directly on the competition between nucleation and wall motion, the number of nuclei sites and the Barkhausen volume. The interest in quantifying these parameters appears to be evident.

IV. APPLICATION TO THE Au/Co/Au SANDWICHES

We apply our model to investigate the magnetic reversal of a cobalt ultrathin layer. We shall show that a dynamical study of hysteresis loops performed by surface magneto-optical Kerr effect with a field variation rate up to 1.2 mOe/s (for experimental device, see Ref. 8) and an analysis of the data based on our calculations, allows us to define the main reversal process and to quantify the Barkhausen volume, the nucleation rate, the wall motion, the number, and the radius of nuclei sites.

Our Au(40 nm)/Co(0.8 nm)/Au(3 nm) sandwiches, elaborated in an ultrahigh-vacuum preparation chamber and deposited on a natural molybdenite (MoS_2) (for preparation and structural studies, refer to Refs. 17 and 18) may be considered as a model system to investigate the magnetization reversal phenomenon: in changing the temperature and the deposition rate, and in varying the conditions of annealing of the gold buffer, we obtain drastic changes of the coercive field value and of the shape of the hysteresis loops. Such variations are linked to the magnetic properties of the magnetization reversal varying with the structural quality of the layer. We focus our dynamical study on two MoS_2/Au(40 nm)/Co(0.8 nm)/Au(3 nm) samples: sample I is elaborated at room temperature with a thermal annealing of the gold buffer at 350 °C. For sample II, the 40 nm gold layer is first deposited at 250 °C with a deposition rate of one atomic plane per minute. In both cases, the cobalt layer and the gold overlayer are elaborated at room temperature.

The measurements by polar Kerr effect on sample I are sketched in Figs. 2(a) and 2(b): Fig. 2(a) shows the magnetization in a negative field for several field variation rates (open circles) and, in Fig. 2(b) are plotted the corresponding coercive field versus logarithm of dH/dt. First of all, we notice that the quite linear variation of H_c, all over the dH/dT range, implies that the increase of the coercive field is a direct consequence of aftereffects without modifications of the reversal process with the dH/dt values.[8] By using the analytical expression of the magnetization Eq. (20) depending on dH/dt, we compare our theoretical results to the experimental data, adjusting the five intrinsic parameters: V, R_0, V_0, N_0, and r_c. Even if a fit is usually perilous with too many unknown variables, we avoid this uncertainty by realizing the fitting procedure on each magnetization curve corresponding to a specific dH/dt values. As the parameters defined above are intrinsic properties of the sample, the validity of the modelization implies to find constant values whatever dH/dt.

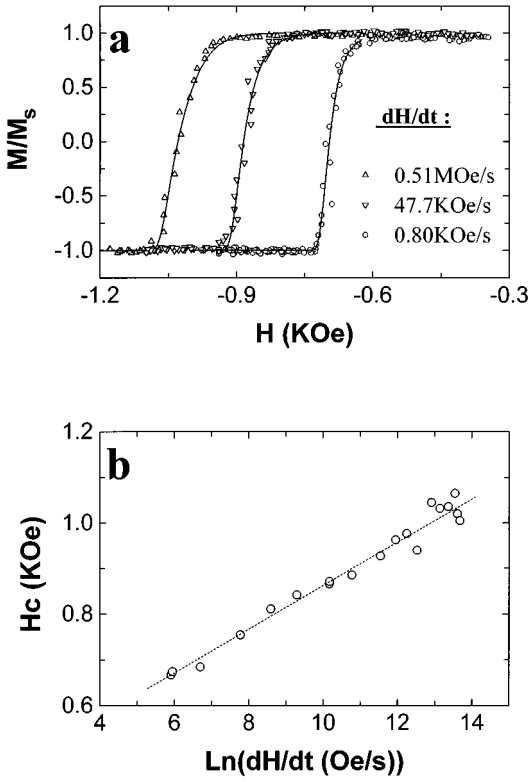

FIG. 2. Hysteresis loops at 300 K of Au/Co(0.8 nm)/Au sandwich (Sample I) obtained from Kerr rotation and analysis from Eq. (20). (a) Perpendicular hysteresis loops for several field variation rate (dH/dt). Experimental data (open circles) and theoretical curves (full lines); (b) plot of the corresponding coercive field H_c versus the logarithm of dH/dt. The dashed line is a guide for eyes.

TABLE I. Values of V, R_0, V_0, r_c, and N_0, obtained by fitting the experimental Kerr-effect data of Sample I, for several values of dH/dt and using Eq. (20).

dH/dt (Oe/s)	V (10^{-19} cm^3)	R_0 (10^{-10} s^{-1})	V_0 (10^{-15} cm/s)	r_c (10^{-6} cm)	N_0 (10^8)	k
381	10.3	9.7	1.49	1.89	1.84	
804	10.5	9.42	1.49	1.82	1.98	
5380	9.83	8.83	1.44	1.83	2.09	
10 964	9.5	10.1	1.1	1.94	2.1	
26 000	9.59	9.85	1.5	1.83	2.0	
47 700	9.55	12.1	1.3	1.9	2.05	
103 600	9.35	10.6	1.03	1.98	2.24	
209 200	9.09	10.0	1.48	1.82	2	
510 000	8.86	10.3	1.44	1.83	2.01	
763 200	8.64	10.2	1.5	1.79	2.03	
815 500	9.07	10.1	1.48	1.79	2.01	
874 000	9.26	10.2	1.43	1.79	2.01	
Average	9.46	10.1	1.39	1.85	2.03	0.75

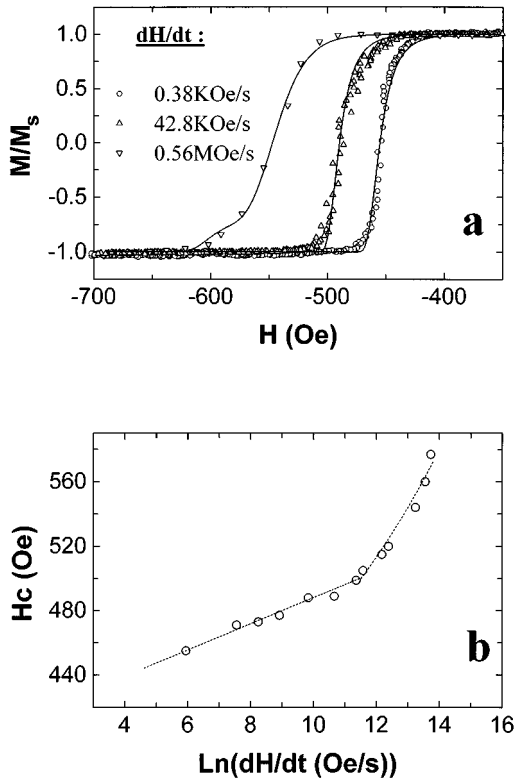

FIG. 3. Hysteresis loops at 300 K of Au/Co(0.8 nm)/Au sandwich (Sample II) obtained from Kerr rotation and analyzed from Eq. (20). (a) Perpendicular hysteresis loops for several field variation rate (dH/dt). Experimental data (open circles) and theoretical curves (full lines); (b) plot of the corresponding coercive field H_c versus the logarithm of dH/dt. The dashed line is a guide for eyes.

The theoretical curves from Eq. (20) and the experimental measurements are given in Fig. 2(a). From their fitting, the V, R_0, V_0, N_0, and r_c values are deduced and reported in Table I. An excellent agreement between the experimental (open circles) and calculated (full line) loops (only the negative field is presented) is observed. The weak dispersion of the V, R_0, V_0, N_0, and r_c values insures the validity of the investigation. The average Barkhausen volume is about 0.95×10^{-18} cm^3, which corresponds to a 35 nm characteristic interfacial length L_b in the magnetic layer. From the deduced R_0 and V_0 values, we derive the analytical expression of $V(H)$ and $R(H)$; besides, we evaluate the ratio k, $k\cong0.75$. That means that both nucleation and wall motion take part in the reversal process. Reported to the unit of area, the total number of nuclei is about to 2×10^{10} cm^{-2} and the calculated value α ($\alpha\cong0.23$) confirms the mixed behavior of the magnetization.

Let us underline that we attempted unsuccessfully to study these dynamical measurements, using our previous works developed elsewhere.[8] This unsuccess arises from the fact that the precedent phenomenological approach cannot take into account, simultaneously, the nucleation and the wall motion processes, contrary to our actual modelization. We conclude that the main interest of our calculation is that it works for mixed regimes which are the general cases. The microscopic parameters can be defined just by studying the magnetization reversal by dynamical Kerr-effect measurements.

Figures 3(a) and 3(b) show the polar Kerr results obtained in sample II. The drastic transition observed on the variation of H_c versus $\ln(dH/dt)$ [Fig. 3(b)] and the widening of the magnetization reversal [Fig. 3(a)] in high dH/dt values (open circles) emphasize an original dynamical effect occurring in the switch of the magnetization. We first mention this behavior in a previous paper[8] and we assumed that, beyond a critical field variation rate, the nucleation might be predominant. In Fig. 3(a) (full lines) and in Table II are reported the fitting results of the experimental data, using Eq. (20). We unambiguously establish that below 180 kOe/s, the main mechanism is the wall motion ($k\cong9$) with a Barkhausen volume of 2×10^{-18} cm^3. For a 190 kOe/s dH/dt value, one observes a transition through the variations of the R_0 and V_0 values (increase of R_0 and decrease of V_0, Table II). In the range of higher field variation rate, the narrow distribution of the parameters and the evaluated ratio k, equal to 5×10^{-3} improve the nucleation to be the main process. In addition, the corresponding theoretical curves are perfectly adjusted to the experimental measurements, in the range of low and high dH/dt values. Let us specify that, in a logical way, we find the Barkhausen volume, the number, and the

TABLE II. Values of V, R_0, V_0, r_c, and N_0, obtained by fitting the experimental Kerr-effect data of Sample II, for several values of dH/dT and using Eq. (20).

dH/dt (Oe/s)	V (10^{-18} cm^3)	R_0 (10^{-13} s^{-1})	V_0 (10^{-17} cm/s)	r_c (10^{-6} cm)	N_0 (10^8)	k
381	1.94	3.77	1.45	4.31	3.15	
1898	1.97	3.73	1.44	4.33	3.17	
3796	2.01	3.7	1.4	4.32	3.11	
42 800	2.09	3.75	1.4	4.42	3.03	
85 840	2.9	3.75	1.42	4.42	3	
Average	2.02	3.73	1.42	4.35	3.08	9
193 600	2.01	3.79×10^2	1.43×10^{-1}	4.31	3.1	
562 000	1.89	1.6×10^2	3×10^{-2}	4.4	3.94	
767 400	1.86	1.2×10^2	6.2×10^{-2}	3.5	4.27	
914 400	1.8	3.72×10^2	4.56×10^{-2}	4.5	3.49	
Average	1.85	2.19×10^2	4.58×10^{-2}	4.13	3.9	510^{-3}

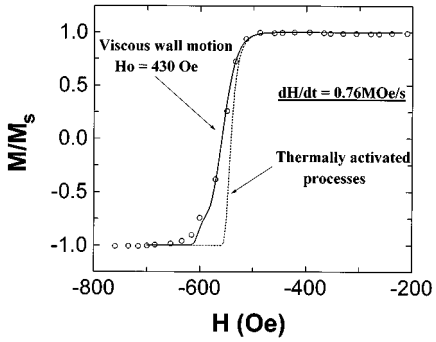

FIG. 4. Fit of perpendicular Kerr effect of Au/Co(0.8 nm)/Au sandwich (Sample II) performed at 300 K with $dH/dt=0.76$ mOe/s. Experimental data (open circles), theoretical curve taking into account the viscous wall motion [full line, using Eq. (24)] and theoretical curve with only thermally activated processes [dashed line, using Eq. (20)].

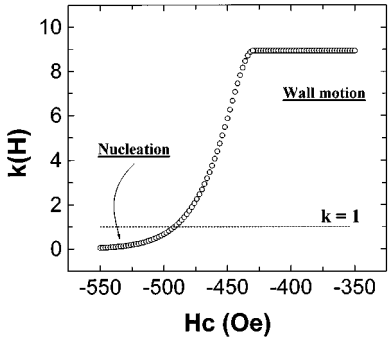

FIG. 5. Plot of the theoretical variation of $k(H)$ as a function of the coercive field H_c, deduced from Eq. (25).

radius of nucleations quite constant, whatever the field frequency.

Nevertheless, one could object that it is physically criticizable to modify the nucleation rate and the wall velocity in zero field versus the range of the field variation rate to adjust the experimental data (Table II). Such an approach just traduces that the magnetic energy given by the variable applied field cannot be stored, *ad infinitum*, by the domain wall. Above a critical field, the exponential law of the wall motion, Eq. (13), exhibits a saturation, the domain-wall changes of propagation regime, and, in high magnetic field, their motion is limited by a theoretical value.[19] One could assume a transfer of the excess energy to the nucleation process, which makes it predominant.

Our calculation, described in Sec. II, only takes into account some thermally activated jumps of the domain wall and the nucleation reversal. In the light of the works devoted to the wall motion measurements in ultrathin magnetic layers,[20,21] we propose to generalize our modelization to some nonthermally activated processes which can occur in high dynamical stimulations: the authors observe that, above a critical magnetic field, the wall displacement leaves the thermally activated regime to a complex viscous motion with a linear variation of the velocity versus the applied field. Therefore, we attempt to modelize the dynamical magnetization using the following expression of the wall motion:

$$V(H)=[1-\theta(H_0-H)]\times V_0\exp(-\beta VM_sH)+\theta(H_0-H)\times V_0\exp(-\beta VM_sH_0)[1-\beta VM_s(H-H_0)], \quad (21)$$

where H_0 is the specific field of the transition between the thermally activated regime [first term of Eq. (21)] and the viscous regime (corresponding to the last term); $\theta(H)$ is the classical unit step function. A straightforward calculation confirms the continuity of the velocity near H_0.

Substituting Eq. (21) in Eq. (9), we obtain a new expression of the switched area $A'[H,(dH/dt)]$, given by

$$A'[H,(dH/dt)]=[1-\theta(H_0-H)]\times A[H,(dH/dt)]+\theta(H_0-H)\frac{N_0\pi}{(dH/dt)T}\int_0^H R(H_1)\exp\left(-\frac{1}{(dH/dt)}\int_0^{H_1}R(H)dH\right)\times\left(\int_{H_1}^{H}\frac{V_0\exp(-\beta VM_sH_0)[1-\beta VM_s(H-H_0)]}{(dH/dt)}dH+r_c\right)^2 dH_1. \quad (22)$$

After integrations and term rearrangement, the above equation is reduced to

$$A'[H,(dH/dt)]=[1-\theta(H_0-H)]\times A[H,(dH/dt)]+\theta(H_0-H)\frac{N_0\pi R_0}{(dH/dt)T}\int_0^H\exp(-\beta VM_sx)\times\exp\left(\frac{R_0}{\beta(dH/dt)VM_s}[\exp(-\beta VM_sx)-1]\right)\frac{V_0\exp(-\beta VM_sH_0)}{(dH/dt)}\times\left[(H-x)-\beta VM_s\left(\frac{H^2}{2}-\frac{x^2}{2}-H_0H+H_0x\right)+r_c\right]^2 dx. \quad (23)$$

This yields to the general expression of the magnetization, taking into account the viscous motion of the domain wall above a critical field:

$$M[H,(dH/dt)]=M_s\Bigg[-2\Bigg(1-\exp\Bigg\{-[1-\theta(H_0-H)]A[H,(dH/dt)]-\theta(H_0-H)\frac{N_0\pi R_0}{(dH/dt)T}\int_0^H \exp(-\beta VM_s x)$$
$$\times\exp\Bigg(\frac{R_0}{\beta(dH/dt)VM_s}[\exp(-\beta VM_s x)-1]\Bigg)\frac{V_0\exp(-\beta VM_s H_0)}{(dH/dt)}$$
$$\times\Bigg[(H-x)-\beta VM_s\Bigg(\frac{H^2}{2}-\frac{x^2}{2}-H_0H+H_0x\Bigg)+r_c\Bigg]^2dx\Bigg\}\Bigg)+1\Bigg]. \quad (24)$$

Using this new equation, we simulate the dynamical behavior of sample II. We observe that, keeping constant the values of V, R_0, V_0, N_0, and r_c defined in the fitting procedure in low-field variation rate [Eq. (20), first part of Table II], we reproduce the dynamical transition around 180 kOe/s, just introducing the viscous displacement of the wall. The only unknown parameter of Eq. (24) is the critical transition field H_0.

We compare the calculated magnetization Eq. (24), to the experimental results (Fig. 4) and we adjust the theoretical curve, by varying H_0. We deduce a critical field of 430 Oe and we obtain a good agreement between the modelization (full line) and the experimental data (open circles). Nevertheless, one remarks that, in high-field variation rate, it is usually difficult to fit the approach to the magnetic saturation. In fact, we assume that the dynamical stimulation increases the effects of a weak distribution of the Barkhausen volume on the hysteresis loop: the dynamical behavior of the wall motion would depend on the size of the jump; a thermally activated regime is supposed to persist in some little volumes. Therefore, a more adjusted fit would imply a distribution of the critical transition field. The dotted line represents the calculated magnetization without considering the viscous wall motion above H_0 [using Eq. (20)]. The large discrepancy with the experimental curve improves the dynamical divergence of the coercive field and the crucial role played by the viscous motion of the domain wall.

We notice that, in low-field variation rate, the viscous behavior of the wall motion does not influence the magnetic transition $+M_S/-M_S$; the transition field H_0 and the H_c values are too close to modify the loop. On the other hand, near the coercive field corresponding to high dH/dt values, the discrepancy between the theoretical exponential law of the velocity (in the case of thermally activated process) and the linear law (for a viscous motion) becomes very large; it implies an additional delay in the magnetic switch, due to the viscous process. Consequently, one observes the divergence of the coercive field and the widening of the $+M_S/-M_S$ transition in high-field variation rate.

Finally, we conclude that considering the nucleation process to become predominant or the viscous wall motion above a critical field, yields satisfactory results. In fact, our interpretation strongly suggests that a delayed propagation of the walls due to a viscous displacement implies a predominant nucleation process. Besides, let us remark that, considering the general expression of the velocity, Eq. (21), the ratio k depends on the magnetic field according to

$$k(H)=\frac{[1-\theta(H_0-H)]\times V_0\exp(-\beta VM_sH)+\theta(H_0-H)\times V_0\exp(-\beta VM_sH_0)[1-\beta VM_s(H-H_0)]}{r_c\times R_0\exp(-\beta VM_sH)}. \quad (25)$$

A simple numerical application, with the parameters defined above, allows us to express the variation of k versus the coercive field. It allows us to observe directly the evolution of the prevailing reversal process with the dynamical stimulation of the sample. The plotted data in Fig. 5 clearly show that, in low-field variation rate (i.e., for low H_c values), the main process is the wall motion. Increasing dH/dt, (i.e., the coercive field), the wall motion mechanism becomes less and less efficient. One observes that the theoretical transition, corresponding to $k\cong 1$, occurs for $H_c\cong 490$ Oe. Compared with the experimental results [Fig. 3(b)], the agreement is rather good.

V. CONCLUSION

The present paper has proposed an original modelization of the magnetization reversal in an ultrathin magnetic layer. An analytical expression of the magnetization is established, considering the after effects due to the dynamic of the applied field and the competition between the wall motion and the nucleation processes.

We have shown that a dynamical study related to our calculation, allows us to define unambiguously the mechanisms of magnetization reversal and to give quantitative information on the nucleation rate, the velocity of the domain wall, the density and the radius of nuclei centers, and the Barkhausen volume.

We have applied our modelization to the magnetization reversal of Au/Co/Au sandwiches. We quantified different reversal processes depending on the structural quality of the sample. In the high dynamic regime, we have observed that the nucleation is usually the most efficient mechanism to switch the magnetization. This original behavior is reason-

ably well taken into account by introducing a viscous wall motion above a critical field.

We conclude that, due to the sharpness of the experimental hysteresis loops, we succeed to fit the magnetization without using any distribution of the activation energy. However, a more realistic approach would consider a weak distribution of the Barkhausen volume, it would imply a distribution of the transition field H_0, depending on the size of the volume. Modelizations extended to spatial inhomogeneities are under development and will be applied to heterogeneous ultrathin magnetic layers.

ACKNOWLEDGMENT

The authors gratefully acknowledge Dr. J. Ferré for helpful discussions.

[1] R. Allenspach, M. Stampanoni, and A. Bischof, Phys. Rev. Lett. **65**, 3344 (1990); R. Allenspach, J. Magn. Magn. Mater. **129**, 160 (1994).

[2] J. Pommier, P. Meyer, G. Pénissard, J. Ferré, P. Burno, and D. Renard, Phys. Rev. Lett. **65**, 2054 (1990).

[3] C. Armand, J. P. Peyrade, R. Mamy, M. D. Ortega, M. Goiran, A. R. Fert, B. Raquet, J. C. Ousset, Phys. Status Solidi B **195**, 167 (1996).

[4] H. P. Oepen, M. Benning, H. Ibach, C. M. Schneider, and J. Kirschner, J. Magn. Magn. Mater. **86**, L137 (1990).

[5] G. Bochi, H. J. Hug, D. I. Paul, B. Stiefel, A. Moser, I. Parashikov, H. J. Güntherodt, and R. C. O'Handley, Phys. Rev. Lett. **75**, 1839 (1995).

[6] Y. Yafet and E. M. Gyorgy, Phys. Rev. B **38**, 9145 (1988); B. Kaplan and G. A. Gehring, J. Magn. Magn. Mater. **128**, 111 (1993); G. A. Gehring and M. Kesking, J. Phys. Condens. Matter **5**, L581 (1993).

[7] P. Bruno, G. Bayreuther, P. Beauvillain, C. Chappert, G. Lugert, D. Renard, J. P. Renard, and J. Seiden, J. Appl. Phys. **68**, 5759 (1990).

[8] B. Raquet, M. D. Ortega, M. Goiran, A. R. Fert, J. P. Redoules, R. Mamy, J. C. Ousset, A. Sdaq, and A. Kmhou, J. Magn. Magn. Mater. **150**, L5 (1995).

[9] E. Fatuzzo, Phys. Rev. **127**, 1999 (1962).

[10] M. Labrune, S. Andrieu, F. Rio, and P. Bernstein, J. Magn. Magn. Mater. **80**, 211 (1989).

[11] M. Avrami, J. Chem. Phys. **7**, 1103 (1939); **8**, 212 (1940); **9**, 177 (1941).

[12] E. Fatuzzo and W. J. Merz, Phys. Rev. **116**, 61 (1959).

[13] D. J. Craik and M. J. Wood, Phys. Status Solidi **16**, 321 (1966); **28**, 407 (1968).

[14] F. Rio, P. Bernstain, and M. Labrune, IEEE Trans. Magn. **Mag-23**, 2266 (1987).

[15] A. Kirilyuk, J. Ferré, J. Pommier, and D. Renard, J. Magn. Magn. Mater. **121**, 536 (1993).

[16] A. Herpin, *Théorie du Magnetisme Bibliotheque des Sciences et Techniques Nucleares* (Presseo Universitaires de France, Saclay, 1968).

[17] R. Mamy, Surf. Sci. **322**, 337 (1995); R. Mamy and B. Carricaburu, J. Phys. Condens. Matter **5**, 6537 (1993).

[18] M. J. Cazanove, E. Snoeck, C. Penchenat, H. Arduin, R. Mamy, B. Raquet, M. D. Ortega, M. Goiran, A. R. Fert, and J. C. Ousset, Thin Solid Films (to be published).

[19] L. R. Walker (unpublished); cf. J. F. Dillon, *Treatise on Magnetism*, edited by G. T. Rado and H. Suhl (Academic, New York, 1963), Vol. III; C. H. Tsang, R. L. White, and R. M. White, J. Appl. Phys. **49**, 6052 (1978); A. P. Malozemoff and J. C. Slonczewski, *Magnetic Domain Walls in Bubble Materials* (Academic, New York, 1979).

[20] A. Kirilyuk, Ph.D. thesis, Orsay University, 1993.

[21] J. Ferré (private communication).